TELKOMNIKA, Vol.17, No.6, December 2019, pp.2867~2876
ISSN: 1693-6930, accredited First Grade by Kemenristekdikti, Decree No: 21/E/KPT/2018
DOI: 10.12928/TELKOMNIKA.v17i6.12852

Performance analysis of high-k materials as stern layer in ion-sensitive field effect transistor using commercial TCAD

Ahmed M. Dinar*[1], AS Mohd Zain[2], F. Salehuddin[3], Mowafak K. Mohsen[4], Mothana L. Attiah[5], M. K. Abdulhameed[6]
[1,2,3,4,5,6]Faculty of Electronics and Computer Engineering, Universiti Teknikal Malaysia Melaka (UTeM), Malacca, Malaysia
[1]Computer Engineering, University of Technology, Baghdad, Iraq
*Corresponding author, e-mail: aealzubydi@gmail.com

Abstract

High-k materials as a STERN Layer for Ion-Sensitive-Field-Effect-Transistor (ISFET) have improved ISFET sensitivity and stability. These materials decrease leakage current and increase capacitance of the ISFET gate toward highest current sensitivity. So far, many high-k materials have been utilized for ISFET, yet they were examined individually, or using numerical solutions rather than using integrated TCAD environment. Exploiting TCAD environment leads to extract ISFET equivalent circuit parameters and performs full analysis for both device and circuit. In this study we introduce a comprehensive investigation of different high-k material, Tio_2, Ta_2O_5, ZrO_2, Al_2O_3, HfO_2 and Si_3N_4 as well as normal silicon dioxide and their effects on ISFET sensitivity and stability. This was implemented by developing commercial Silvaco TCAD rather than expensive real fabrication. The results confirm that employing high-k materials in ISFET outperform normal silicon dioxide in terms of sensitivity and stability. Further analysis revealed that Titanium dioxide showed the highest sensitivity followed by two groups HfO_2, Ta_2O_5 and ZrO_2, Al_2O_3 respectively. Another notable exception of Si_3N_4 that is less than other materials, but still have higher sensitivity than normal silicon dioxide. We believe that this study opens new directions for further analysis and optimization prior to the real cost-ineffective fabrication.

Keywords: *high-k materials, ISFET sensitivity, stern layer, titanium dioxide*

1. Introduction

There has been a tremendous convergence in the last decade in chemical sensing applications, with CMOS-based micro-technology playing a crucial role in this field. This has been enabled using solid-state sensors that can be implemented in planar form and manufactured using CMOS technology to monolithically integrate on a single chip. This technology now provides an opportunity for chemical sensing platforms to leverage semiconductor technology that may offer advantages such as scalability, miniaturisation, fabrication, and integration with intelligent instrumentation. ISFET sensors are the most promising and may satisfy all these opportunities. The essential property of ISFETs is scalability with the developing semiconductor fabrication. This property provides a continuous trend of sensor minimisation, with resulting advantages for biochemical tests, e.g. fast response and the small volume of analyte solution required. Due to its promising application in biological, biochemical and medical detection [1-5], ISFET has received much interest since it was first reported by Bergveld in 1972 [6]. Particularly, much effort has been made to investigate pH sensitive ISFETs with studies on device structures and pH-sensing membranes aimed at improving the sensitivity and stability of ISFETs [7, 8].

Utilizing Gouy–Chapman–Stern model can improve ISFET sensitivity and stability using Stern layer in direct contact with electrolyte in ISFET sensing window. It is well known that the gate dielectric is in direct contact with the electrolyte solution, which determines the starting sensitivity of these devices. As the SiO2 gate dielectric shows a low response sensitivity and poor stability, other inorganic materials such as Al_2O_3 [7, 8], Si_3N_4 [6, 9], Ta_2O_5 [9-11], HfO_2 [12–15] and ZrO_2 [12-14] with their enhanced stability and sensitivity have also been investigated.

Received April 5, 2019; Revised July 2, 2019; Accepted July 18, 2019

The pervious works of using high-k materials as an ISFETs gate used numerical or mathematical modeling simulations [16-19]. However, now that the ISFET has become the mainstream device of a few CMOS-based sensing platforms, accurate and versatile numerical device simulations in an integrated TCAD environment are desirable to support the ISFET design, extract the ISFET equivalent circuit parameters, and perform mixed device-circuit analysis. Also, the previous investigations that used a TCAD environment for high-k gated ISFET while some of them treat it as MOSFET [20], others using new methodology for electrolyte/insulator interfacing [21, 22], but remain challenged to comprehensive investigation for all commonly used high-k materials as an ISFET sensing membrane.

In this study we introduce a comprehensive investigation of different high-k material, TiO_2, Ta_2O_5, ZrO_2, Al_2O_3, HfO_2 and Si_3N_4 as well as normal silicon dioxide and their effects on ISFET sensitivity and stability. This was implemented by developing commercial Silvaco TCAD rather than expensive real fabrication. We believe this study opens new directions for further analysis and optimization prior the real and cost-effective fabrication way.

2. Material and Methods

2.1. Surface Potential Model

Surface charge density that makes the ISFET sensitive to pH is caused by chemical reactions between the ISFET gate dielectric on one side and the electrolyte on the other side [14, 15]. As a first step toward the development of a general methodology, we will chemically and mathematically improve this relationship. Chemically, when we choose the insulator material as a sensing membrane, ions will rest on the surface membrane of the insulator according to the pH concentration. Therefore, the surface potential (ψ_o) is calculated by the hydrogen ion H^+ exchange between electrolyte solution and site binding of an insulator. The pH sensitivity of good insulator should cover wide range of pH scale besides liner response to this range [23]. Mathematically, for an FET device:

$$V_G = V_{FB} + \frac{qN_A X_{d,T}}{C_{OX}} + \frac{qN_A (X_{d,T})^2}{2\varepsilon_s} \quad (1)$$

where V_G is the gate voltage, V_{FB} is flatband voltage, q is electronic charge, N_A is density of concentration, C_{OX} is the insulator capacitance per unit area calculated by $C_{OX}={}^{\varepsilon_{ox}}/_{t_{ox}}$, and $X_{d,T}$ is the depletion layer width that can be found by the following:

$$X_{d.T} = \sqrt{\frac{4\,\varepsilon_s \emptyset_F}{q\,N_a}} \quad (2)$$

where; $\emptyset_F$=semiconductor work function = $\frac{K\,T}{q}\,\ln\frac{N_a}{n_i}$ (3)

Assume that: n_i=1.43 e^{10} cm^{-3} for silicon, and n_i=1.92 e^{16} cm^{-3} for high-k material. Therefore, $\emptyset_F$=4.17 eV for silicon and 4.59 eV for high-k material. The previous equation shows that we can obtain different V_{FB} values for different V_G values. For ISFET device, we can rewrite (1) as follows [24]:

$$V_{th}^T = E_{ref.} - \psi_o + \chi^{sol} - \frac{Q_{Si}}{q} - \frac{Q_{ox}+Q_{SS}}{C_{ox}} \quad (4)$$

where E_{ref} , χ^{sol}, Q_{Si} , and Q_{ox} are reference electrode potential, electrolyte–insulator interface dipole, work function of silicon, and charge located in the oxide, respectively. Q_{SS} and C_{ox} are equivalent insulator–silicon interface charge and top-insulator capacitance per unit area, respectively. As mentioned in Section 1, the surface potential ψ_o modulates the floating gate and shifts ISFET threshold voltage V_T .Therefore, the Nernst equation control the proton activity at interface area that relates to potential is written as follows [25]:

$$\psi_o = \frac{kT}{q}\ln\frac{aH^+_{bulk}}{aH^+_{Surface}} \quad (5)$$

where *q* and *k* are elementary charge and Boltzmann constant, respectively. *a* is the proton activities in gate dielectric–electrolyte interface area and electrolyte. Therefore, we can conclude from (4) and (5) that the shift in threshold voltage for conventional ISFETs is given by the following:

$$V_{th}^{T} = -\Delta\psi_o \tag{6}$$

The site-dissociation model developed by Yates [26] describes the relationship between the change of potential with pH change, as follows:

$$\sigma_0(\psi_0) = qN_{sil}\left[\frac{cH_s^2 - K_a K_b}{cH_s^2 + K_b cH_s + K_a K_b}\right] \tag{7}$$

where

$$cH_s = cH_B exp\left(-\frac{q\psi_0}{kT}\right) \tag{8}$$

where N_{sil} is the number of amphoteric silanol surface sites, and cH_S is the surface H^+ concentration. *Ka* and *Kb* are the surface dissociation constants.

2.2. Electrolyte pH Change Model

As mentioned in section 1, the major challenge is the electrolyte simulation in commercial TCAD because it is not equipped with models, materials, and electrochemical processes that manage ISFET process and its operations [15]. Therefore, our idea exploits the user-defined material property offered by Silvaco to simulate electrolyte solution [27]. The properties of a user-defined material offered by Silvaco are exploited to simulate the electrolyte (solution) behavior. The parameters of silicon semiconductor material (i.e., energy bandgap, permittivity, affinity, and density of states) are reconstructed in an electrolyte solution. Therefore, electrostatic solution of the electrolyte area can be investigated by giving a numerical solution for the semiconductor equation inside this area. Three types of materials are available in Silvaco Atlas, namely, semiconductor, insulator, and conductor. The procedure of defining a new material in Atlas (user-defined) specifies the material name, the user group it belongs to, and the last known atlas about the default material. When these parameters are set in their correct places in the Silvaco input deck code, we can change and manipulate the material properties using material statements (i.e., permittivity, energy bandgap, affinity, and density of states) as is typically done [27].

The most important parameters that bind the electrolyte solution physical properties with the intrinsic semiconductor electrical parameters are density of states, conduction band NC, and valence band NV. These parameters play key roles in the molar concentration of the solution based on the following methodology. At the chemical equilibrium, the dissociation of H2O is (H+ + OH−). Thus, the mass action law at 25°C and pure water is introduced by the following [28]:

$$K_\omega = [H^+]\,[OH^-] \tag{9}$$

$$H^+ = OH^- = 1.0\, e^{-07} mol/L \tag{10}$$

thus,

$$K_\omega = 1.0\, e^{-14} \tag{11}$$

The mass action law states that multiplying the free hole concentration *p* and the free electron *n* is equal to the square of the intrinsic carrier concentration n_i under thermal equilibrium. The carrier concentration can be given as follows, based on Boltzmann statistics [29]:

$$p = N_V\, e^{-\frac{E_f - E_v}{kT}} \tag{12}$$

$$n = N_C e^{-\frac{E_C - E_f}{kT}} \quad (13)$$

where E_V, E_C, and E_f are the upper energy level of the valence band, the lower value level of the conduction band, and the Fermi level, respectively. If $p=[H^+]$, $n=[OH^-]$, and $n=p$ *from (10);* if $E_C-E_f=E_f-E_V=E_g/2$ from [30] Thus, we can rewrite (12) and (13) as follows:

$$N_C = ne^{\frac{E_g}{2kT}} \quad (14)$$

$$N_V = pe^{\frac{E_g}{2kT}} \quad (15)$$

Therefore, (14) and (15) clearly demonstrate the relationship between pH change in electrolyte and the density of state for valence and conduction band. The site-binding model side can be updated based on the relation that described from (9) to (15) by replacing each H^+ with its semiconductor counterpart. The mass action law in (9) is the same as the relation $n_i^2 = np$. Therefore, we can rewrite (7) as follows:

$$\sigma_0 = qN_{sil}\left(\frac{p\, n_i^2 - K_a K_b n}{p\, n_i^2 + K_b\, n_i^2 + K_a K_b n}\right) \quad (16)$$

where the n_i is a constant, and only p and n will change with pH.

2.3. TCAD Simulation

Commercial TCAD allows users to introduce bias-dependent surface charges in the form of interface donor or acceptor traps. The challenge is simulating the updated surface charge density equation described by (16) in the electrolyte pH change model [31]. To introduce this equation to the simulator, interface trap statements are utilized to mimic the surface charge accurately, as follows [27]:

INTTRAP <type> E. LEVEL= <r> DENSITY= <r> <capture parameters>

"INTTRAP activates interface defect traps at discrete energy levels within the bandgap of the semiconductor and sets their parameter values. Device physics has established the existence of three different mechanisms, which add to the space charge term in Poisson's equation in addition to the ionized donor and acceptor impurities" [27]. Interface traps will add space charge directly into the right-hand side of Poisson's equation. To calculate the trapped charge in Poisson's equation, the total charge value is defined by the following:

$$\sigma_0 = q(N_{tD}^+ - N_{tA}^-) \quad (17)$$

where N_{tD}^+ and N_{tA}^- are the densities of ionized donor-like and acceptor-like traps, respectively. DENSITY and its probability of ionization are represented as *FtA* and *FtD*, respectively. For donor-like and acceptor-like traps, the ionized densities are calculated by the following equations:

$$N_{tD}^+ = \text{DENSITY} \times F_{tD} \quad (18)$$

$$N_{tA}^- = \text{DENSITY} \times F_{tA} \quad (19)$$

where *FtA* and *FtD* are given by the following equations:

$$F_{tA} = \frac{V_n\, SIGN\ n + e_{pA}}{V_n\, SIGN\ n + V_p\, SIGP\ p + e_{nA} + e_{pA}} \quad (20)$$

$$F_{tD} = \frac{V_p\, SIGP\ p + e_{nD}}{V_n\, SIGN\ n + V_p\, SIGP\ p + e_{nD} + e_{pD}} \quad (21)$$

where *SIGN* is the carrier capture cross sections for electrons and *SIGP* holes. The thermal velocities for electrons and holes are V_n and V_p , respectively. For donor-like traps, the electron and hole emission rates, e_{nD} and e_{pD}, are defined by the following [27]:

$$e_{nD} = \frac{1}{DEGEN.FAC} V_n \, SIGN \, n_i \, e^{E_t - E_i / kT} \quad (22)$$

$$e_{pD} = DEGEN.FAC \, V_p \, SIGP \, n_i \, e^{E_i - E_t / kT} \quad (23)$$

where *Et and Ei are* the trap energy level and the intrinsic Fermi level position, respectively. DEGEN.FAC is the degeneracy factor of the trap center. For acceptor traps, the electron and hole emission rates, e_{nA} and e_{pA} , are defined by the following [27]:

$$e_{nA} = DEGEN.FAC \, V_n \, SIGN \, n_i \, e^{E_t - E_i / kT} \quad (24)$$

$$e_{pA} = \frac{1}{DEGEN.FAC} V_p \, SIGP \, n_i \, e^{E_i - E_t / kT} \quad (25)$$

for example, the acceptor interface trap statement and its parameters are as following:

INTTRAP ACCEPTOR E.LEVEL: DENSITY: INTMATERIAL: DEGEN.FAC EoN: EoP: SIGN: SIGP:

Considering all equations mentioned above, we can rewrite the sit-binding model (1) based on TCAD model. We first assume that acceptor and donor traps exchange carriers only with the conduction and valence band of the semiconductor representing the electrolyte, respectively. Hence, we can rewrite (7) in terms of TCAD model as follows:

$$\sigma_{(TCAD)} = q \times DENSITY \left(\frac{V_P \, SIGP \, P - V_n SIGN \, n}{v_P \, SIGP \, P + V_n SIGN \, n + K_b n_i^2} \right) \quad (26)$$

for more details about TCAD simulation and modelling, the previous work was well described all modelling methodologies [32].

3. Results and discussion

In this section a comparison results of different high-k materials as ISFET sensing membrane will introduce. Table 1 and Table 2 are the TCAD simulation parameters. The parameters required for validation and simulation are easily derived from the literature data as shown in Table 2.

Table 1. TCAD Parameters of ISFET

Parameter	Value	Unit	Parameter	Value	Unit
t_{Stern}		-	Channel length	200	nm
T	300	K	S/D doping	10^{17}	cm^{-3}
k	1.380649×10−23	J/K	S/D length	50	nm
$t_{electrolyte}$	1000	nm	Electrolyte concentration	10^{-3}	Mol/L
t_{ox}	3	nm	Oxide permittivity	3.9	-
Electrolyte permittivity	80	-	V_{DS}	50	mV

The difference in this work with other works and investigations, the research data extracted directly from TCAD as a transfer characteristic. Therefore, the equations from 1 to 26 is interpreted as Silvaco ATHENA and ATLAS codes [27]. An ISFET device is simulated to check the suitability of the modeling procedure. The cross-section of the ISFET simulation structure is shown in Figure 1. The parameters required for validation and simulation for

example SiO_2 gate dielectric to check the validity of our model and to show the agreement of models with the theoretical models and with experimental work. The first set of model validation examines the effect of changing pH on charge density in site-binding model. This is accomplished by comparing our models with the theoretical model developed by Yat [26] as shown in Figure 2. Furthermore, the density of states *NC* and *NV* according to pH change values shown in Figure 3.

Table 2. Materials Parameters used in TCAD Simulation [9, 16, 25]

Material	Dilectric Constant	Density	K_a	K_b
Sio_2	3.9	$5 . 10^{14}$ (1/cm^2)	10^{-6}	10^{2}
Ta_2O5	22	$10 . 10^{14}$ (1/cm^2)	10^{-4}	10^{-2}
TiO_2	80	$1.2 . 10^{14}$ (1/cm^2)	10^{-9}	$2.5 . 10^{-3}$
Si_3N_4	7.5	$3. 10^{14}$ (1/cm^2)	10^{-6}	10^{2}
Al_2O_5	14	$8 . 10^{14}$ (1/cm^2)	10^{-10}	10^{-6}
HfO_2	25	$8 . 10^{14}$ (1/cm^2)	10^{-10}	10^{-6}
ZrO_2	22	$9 . 10^{14}$ (1/cm^2)	$2.8 . 10^{-8}$	$2.25 . 10^{-4}$

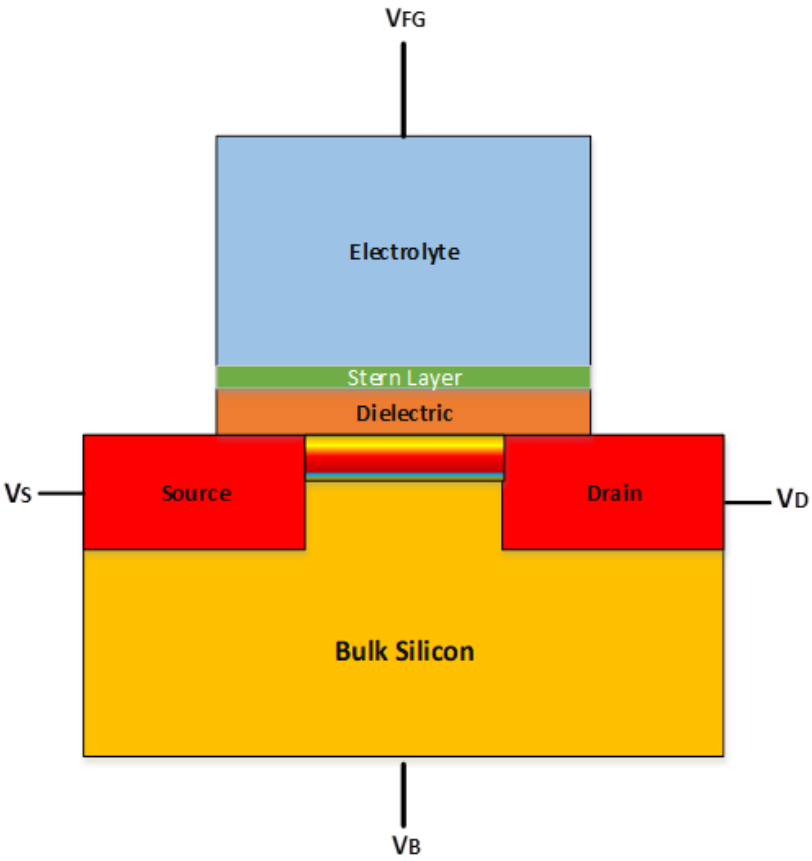

Figure 1. 2D cross section of ISFET

The electrostatic behavior (transfer characteristics) of a conventional ISFET device is simulated. Draining to source current I_{ds} versus the reference gate voltage $V_{Ref.}$ at various pH values for Tio_2, Ta_2O_5, ZrO_2,Al_2O_3,HfO_2 and Si_3N_4 Stern Layer is shown in Figures 4 (a-f). The observed increase in threshold voltage could be attributed to the increase in pH values. Figures 4 (a-f) shows that the lowest and the highest values of pH report less sensitivity compared with values in the range pH 5–9, which is consistent with the theories [9].

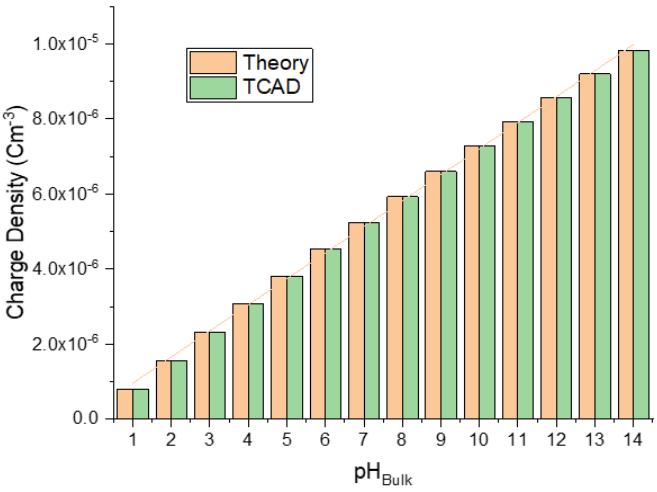

Figure 2. Comparison between the TCAD model and theoretical sit-binding model

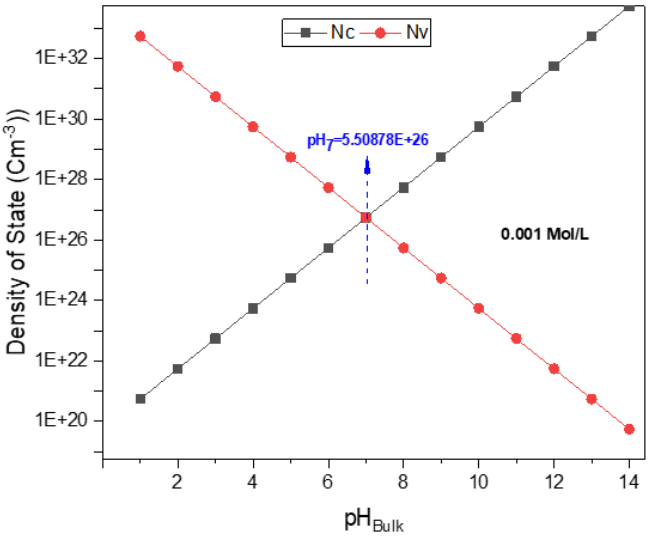

Figure 3. Variation of density of state of valence and conductance band according to pH change

For more analysis, the average sensvity of conventinal Stern-ISFET for Six high-k materials sensing membarane is compared with each as well as the average snestivity of SiO_2 introduced in Figure 5. As shown the high-k sensing membranes are hit the Nearnst limit and the stability also contributed in acceptible way comparing with normal silicon deoxide. Figure 6 discribe the shift in threshold voltage in front of pH bulk change fron 1→14. Slitly diffrence between high-k materials comparing with normal silicon deoxide and the stability of them are reach extremly by 99.99%.

Specifically, the contribution of each sensing membrane from the theoratical snestivity based on Nearnst equation observed in Figure 7. As shown, the most contributed one is TiO_2 by 59.065 mV/pH, next two materials are HfO_2 and Ta_2O_5 by ~59.03 mV/pH. The lowest two materials are ZrO_2 and Al_2O_3 by 59.007 mV/pH and 59.02 mV/ph, respectivily. Finally, Si_3N_4 is notable exception as shown because of the SiOH groups formed by oxidation of silicon, the Si_3N_4 surface is characterized by additional basic sites formed by primary amine groups [10].

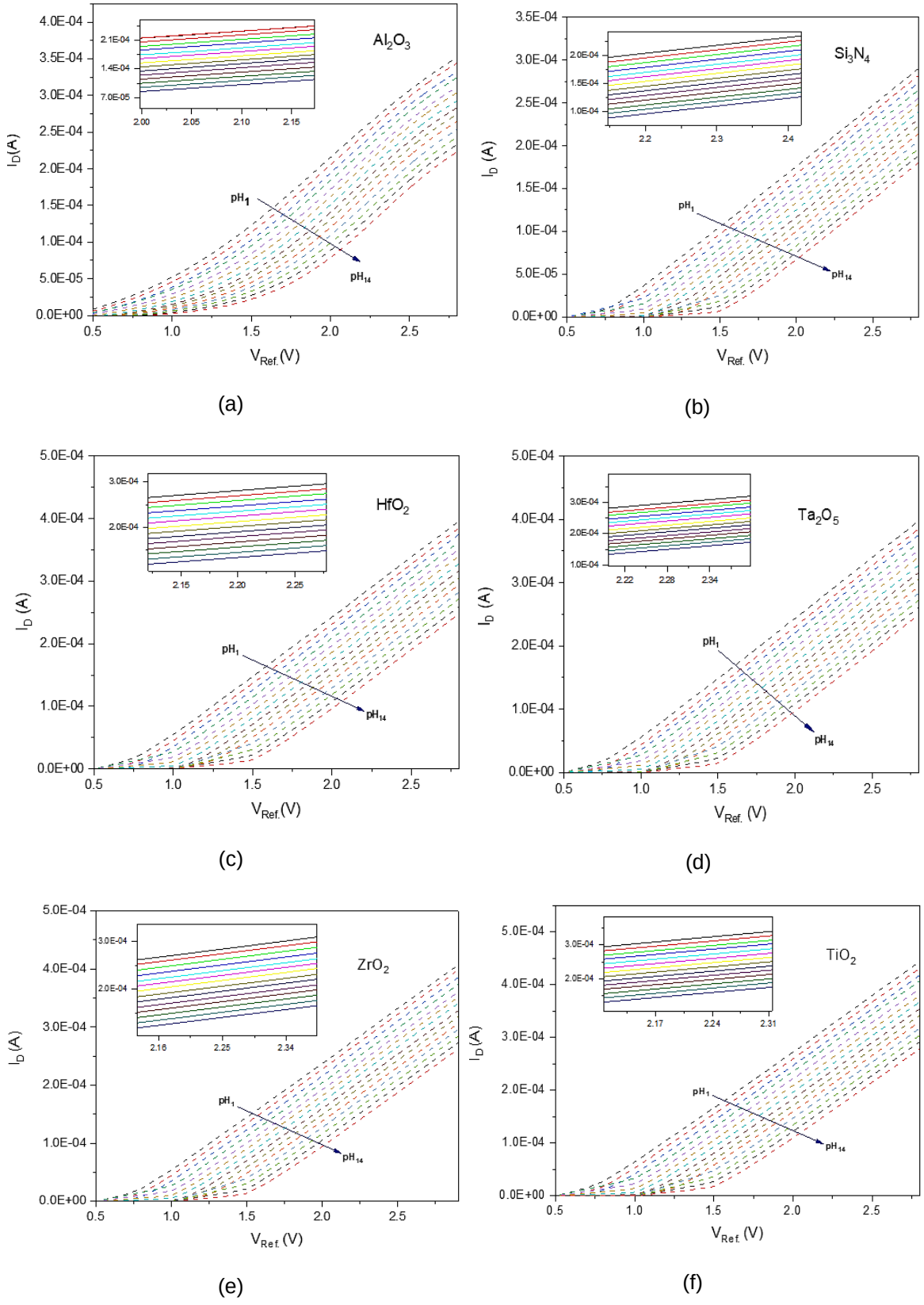

Figure 4. Transfer characteristics with respect to the reference gate voltage for the Sensing Membranes as ISFET stern layer, (a) Al_2O_3, (b) Si_3N_4, (c) HfO_2, (d) Ta_2O_5, (e) ZrO_2, (f) Tio_2

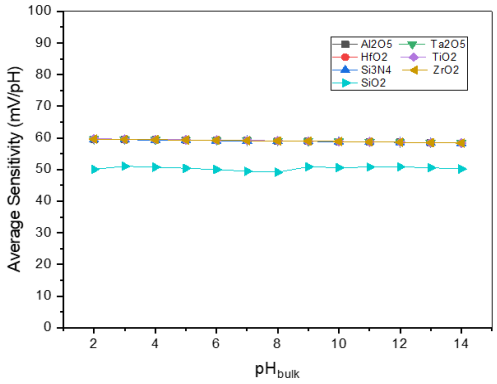

Figure 5. Average sensitivity of all sensing Membaranes with Sio_2

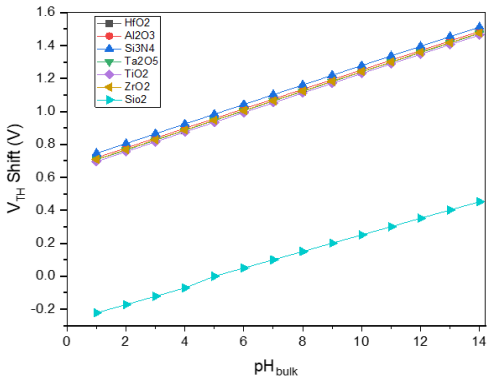

Figure 6. TCAD simulation threshold voltage shift of all sensing membaranes with Sio_2

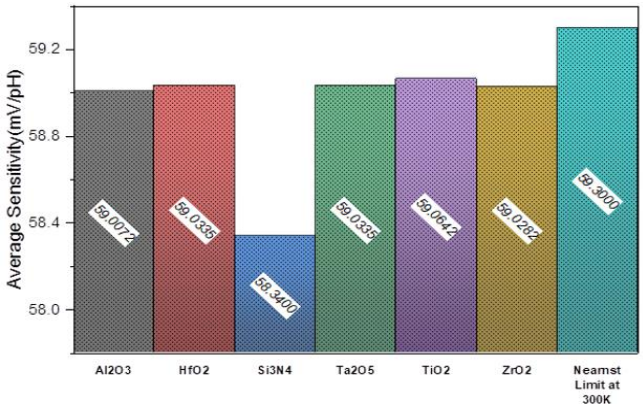

Figure 7. Average sensitivity of all sensing membaranes with nearnst limit

4. Conclusion

In this study we introduce a comprehensive investigation of different high-k material as well as normal silicon dioxide and their effects on ISFET sensitivity and stability. This was implemented by developing commercial Silvaco TCAD rather than expensive real fabrication. The results confirm that employing high-k materials in ISFET outperform normal silicon dioxide in terms of sensitivity and stability. Further analysis revealed that Titanium dioxide showed the highest sensitivity followed by two groups HfO_2, Ta_2O_5 and ZrO_2, Al_2O_3 respectively. Further studies should investigate the performance analysis of commonly used high-k materials using same approach. Although the simulation approach still considered not real fabrication and measurements, this study opens new directions for further analysis and optimization prior the real and cost-effective fabrication way.

Acknowledgments

The authors gratefully acknowledge the UTeM Zamalah Scheme, Universiti Teknikal Malaysia Melaka (UTeM), and the supports from the Centre for Research and Innovation Management (CRIM), Centre of Excellence, Universiti Teknikal Malaysia Melaka (UTeM).

Reference

[1] A Bratov, N Abramova, C Domínguez. Investigation of chloride sensitive ISFETs with different membrane compositions suitable for medical applications. *Anal. Chim. Acta*. 2004; 514(1): 99-106.
[2] CS Lee, S Kyu Kim, M Kim. Ion-sensitive field-effect transistor for biological sensing. *Sensors*. 2009; 9(9): 7111–7131.
[3] T Sakurai, Y Husimi. Real-Time Monitoring of DNA Polymerase Reactions by a Micro ISFET pH Sensor. *Anal. Chem.* 1992; 64(17): 1996–1997.

[4] AM Dinar, ASM Zain, F Salehuddin. CMOS ISFET device for DNA Sequencing : Device Compensation, Application Requirements and Recommendations. *Int. J. Appl. Eng. Res.* 2017; 12(21): 11015–11028.
[5] AM Dinar, ASM Zain, F Salehuddin. Utilizing Of Cmos Isfet Sensors In Dna Applications Detection: A Systematic Review. *Jour Adv Res. Dyn. Control Syst.* 2018; 10(4): 569–583.
[6] P Bergveld. Development, operation, and application of the ion-sensitive field-effect transistor as a tool for electrophysiology. *IEEE Trans. Biomed. Eng.* 1972; 19(5): 342–351.
[7] MN Niu, XF Ding, QY Tong. Effect of two types of surface sites on the characteristics of Si3N4-gate pH-ISFETs. *Sensors Actuators B Chem.* 1996; 37(1–2): 13–17.
[8] S Chen, JG Bomer, ET Carlen, A Van Den Berg. Al2O3/silicon nanoISFET with near ideal nernstian response. *Nano Lett.* 2011; 11(6): 2334–2341.
[9] REG Van Hal, JCT Eijkel, P Bergveld. A general model to describe the electrostatic potential at electrolyte oxide interfaces. *Adv. Colloid Interface Sci.* 1996; 69(1–3): 31–62.
[10] DL Harame, LJ Bousse, JD Shott, JD Meindl. Ion-Sensing Devices with Silicon Nitride and Borosilicate Grlass Insulators. *IEEE Trans. Electron Devices*. 1987; 34(8): 1700–1707.
[11] DH Kwon, BW Cho, CS Kim, BK Sohn. Effects of heat treatment on Ta2O5 sensing membrane for low drift and high sensitivity pH-ISFET. *Sensors Actuators B Chem.* 1996; 34(1–3): 441–445.
[12] T Akiyama, Y Ujihira, Y Okabe, T Sugano, E Niki. Ion-Sensitive Field-Effect Transistors with Inorganic Gate Oxide for pH Sensing. *IEEE Trans. Electron Devices*. 1982; 29(12): 1936–1941.
[13] HR Thakur, G Keshwani, JC Dutta, C Engineering. Sensitivity of Carbon Nanotube Based Junctionless Ion Sensitive Field Effect Transistor (CNTJLISFET) for HfO2 and ZrO2 gate dielectrics: *Experimental and Theoretical Investigation*. 2017: 137–142.
[14] V. Jankovic and J. P. Chang. HfO2 and ZrO2–Based Microchemical Ion Sensitive Field Effect Transistor (ISFET) Sensors: Simulation & Experiment. *J. Electrochem. Soc.* 2011; 158(10): 115-P117.
[15] A Tarasov *et al.*. Understanding the electrolyte background for biochemical sensing with ion-sensitive field-effect transistors. *ACS Nano*. 2012; 6(10): 9291–9298.
[16] TM Abdolkader, AG. Alahdal. Performance optimization of single-layer and double-layer high-k gate nanoscale ion-sensitive field-effect transistors. *Sensors Actuators, B Chem.* 2018; 259: 36–43.
[17] G Massobrio, S Martinoia. Modelling the ISFET behaviour under temperature variations using BIOSPICE. *Electron. Lett.* 2002; 32(10): 936-938.
[18] A Podolska *et al.*. Method to Predict and Optimize Charge Sensitivity of Ungated AlGaN/GaN HEMT-Based Ion Sensor Without Use of Reference Electrode. *IEEE Sens. J.* 2015; 15(9): 5320–5326.
[19] AM Dinar, AS Mohd Zain, F Salehuddin. Comprehensive identification of sensitive and stable isfet sensing layer high-k gate based on isfet/electrolyte models. *Int. J. Electr. Comput. Eng.* 2019; 9(2): 926–933.
[20] R Mukhiya *et al.*. Fabrication and characterisation of Al gate n-metal–oxide–semiconductor field-effect transistor, on-chip fabricated with silicon nitride ion-sensitive field-effect transistor. *IET Comput. Digit. Tech.* 2016; 10(5): 268–272.
[21] A Bandiziol, P Palestri, F Pittino, D Esseni, L Selmi. A TCAD-based methodology to model the site-binding charge at ISFET/electrolyte interfaces. *IEEE Trans. Electron Devices*. 2015; 62(10): 3379–3386.
[22] B Choi *et al.*. TCAD-based simulation method for the electrolyte-insulator-semiconductor field-effect transistor. *IEEE Trans. Electron Devices*. 2015; 62(3): 1072–1075.
[23] MJ Spijkman *et al.*. Dual-gate organic field-effect transistors as potentiometrie sensors in aqueous solution. *Adv. Funct. Mater.* 2010; 20(6): 898–905.
[24] JC Chou, LP Liao. Study on pH at the point of zero charge of TiO2pH ion-sensitive field effect transistor made by the sputtering method. *Thin Solid Films*. 2005; 476(1): 157–161.
[25] HJ Jang, WJ Cho. Fabrication of high-performance fully depleted silicon-on-insulator based dual-gate ion-sensitive field-effect transistor beyond the Nernstian limit. *Appl. Phys. Lett.* 2012; 100(7).
[26] W Healy, DE Yates, S Levine. Site-binding Model of the Electrical Double Layer at the Oxide/Water Interface. *Trans. Farad. Soc. I*. 1974; 70: 1807-1818.
[27] DS. Software. ATLAS User's Manual. 2016; 408: 567–1000.
[28] P Fromherz, A Offenhäusser, T Vetter, J Weis. A Neuron-Silicon Junction: A Retzius Cell of the Leech on an Insulated-Gate Field-Effect Transistor. *Science*. 1991; 252(5010): 1290–1293.
[29] D Passeri, A Morozzi, K Kanxheri, A Scorzoni. Numerical simulation of ISFET structures for biosensing devices with TCAD tools. *Biomed. Eng. Online*. 2015; 14(2): 1–16.
[30] RF Pierret. Semiconductor Device Fundamentals. New York. 1996: 792.
[31] E Mohammadi, N Manavizadeh. *Performance and sensitivity analysis of Dual-gated ion sensitive FET*. 2017 25th Iran. Conf. Electr. Eng. ICEE 2017, no. ICEE20 17. 2017: 440–444.
[32] AM Dinar, A Mohd Zain, F Salehuddin, ML Attiah, MK Abdulhameed, MK Mohsen. *Modeling and simulation of electrolyte pH change in conventional ISFET using commercial Silvaco TCAD*. in IOP Conference Series: Materials Science and Engineering. 2019; 518: 042020.